Nonlinear Optical Fibers for Electro-optic Applications

Won-Taek Han and Bok Hyeon Kim*

Department of Information and Communications, School of Photon Science and Technology
Gwangju Institute of Science and Technology (GIST), Gwangju 500-712, Korea
E-mail: wthan@gist.ac.kr
** Advanced Photonic Research Center (APRI), Gwangju Institute of Science and Technology (GIST)*
Gwangju 500-712, Korea
E-mail: bhkim@gist.ac.kr

Abstract: Fabrication and electro-optic applications of glass optical fibers were reviewed. Theoretical description on the electro-optic Kerr effect in glass optical fibers, particularly for the second-order optical nonlinearity was given. Fabrication procedure and the characterization of the nonlinear electro-optic fibers with internal electrodes were described. Several electro-optic devices based on the polarimetric cells made by the nonlinear optical fibers with internal electrodes were also discussed with the experimental results on the electro-optic effect.

1. Introduction

Glass optical fiber is an essential component in the high speed optical communication and sensing systems since it has advantages such as extremely small optical attenuation, high speed and large capacity data transmission, and low fabrication cost. Much attention has been paid to enhance the electro-optic effect of glass optical fiber for device applications since the attractive observation of the strong second-order phenomenon in the fiber[1]. It is well known that a glass doesn't possess any intrinsic electro-optic effect because glass as an amorphous material has the isotropic structural characteristics with the inversion symmetry. However, the large second-order nonlinearity, $\chi^{(2)}$, of 1-12 pm/V in glass fibers was found to be induced, if special treatments were applied to the fibers, such as glass poling accompanied with heat-treatment[2,3] or UV irradiation[4].

Up to now, most applications of the electro-optic fibers and the planar waveguides have been studied with the structure based on a Mach-Zehnder interferometer (MZI)[3,5-9]. Electro-optic data conversion at the rate of 10 MHz for video signal transmission was demonstrated with all-fiber modulator based on the electro-optic fibers[6]. An electro-optically tunable mode-lock laser made by an all- fiber electro-optic modulator was demonstrated[5]. Recently, an electro-optically controlled all fiber polarization controller with fast response time was also examined[7]. In the all-fiber electro-optic devices, the electric-field induced optical phase change in electro-optic fiber used as the active arm of the MZI was basically used to introduce the optical modulation, the tuning, and polarization control.

Based on our previous study, the simply configured polarimetric cells with the electro-optic fibers could be alternatively used for electro-optic modulation[10,11], tuning[12], and control of polarization state[13], even though the polarization dependence of the electric field induced phase change was not so significant in the fibers[7,10]. The electro-optic devices using several polarimetric cells based on the electro-optic fiber with internal electrodes were reviewed and the operating mechanism and the modulation characteristics were also described.

1.1 Electro-optic Kerr effect in glass optical fibers

Generation of the electro-optic effect in glass can be theoretically explained using the nonlinear optical process in glass applied with the electric field. The polarization density, P, of glass under the electric field, E, can be expressed by the series form of the electric susceptibility tensor

$$P_i(E) = \sum_j \varepsilon_0 \chi_{ij}^{(1)} E_j + \sum_{j,k} \varepsilon_0 \chi_{ijk}^{(2)} E_j E_k + \sum_{j,k,l} \varepsilon_0 \chi_{ijkl}^{(3)} E_j E_k E_l + \cdots . \quad (1)$$

where $\varepsilon_0 = 8.85 \times 10^{-12}\ C^2/N \cdot m^2$ is the electric permittivity of free space and χ with the superscripts, $^{(1)}$, $^{(2)}$, and $^{(3)}$ indicate the linear, the second-order, and the third-order nonlinear coefficients, respectively. The equation can be simplified in the scalar form,

$$P(E) = \varepsilon_0 \chi^{(1)} E + \varepsilon_0 \chi^{(2)} E^2 + \varepsilon_0 \chi^{(3)} E^3 + \cdots . \quad (2)$$

In the case that the electric field is very weak, the high order terms can be ignored because the magnitudes of the terms are much smaller than that of the linear term. If the strong electric field is applied, the high order terms become prominent, thus, the terms cannot be neglected.

If the electric field of an optical signal, E_ω, with the field intensity of E_0 and the frequency of ω superimposed on the DC electric field with the magnitude, E_{dc}, is considered as follows,

$$E = E_{dc} + E_\omega = E_{dc} + E_0 \cos \omega t , \quad (3)$$

the polarization density, P_ω, with frequency, ω, is given by[14,15]

$$P_\omega = \varepsilon_0 \chi_{eff} E_0 \cos \omega t = \varepsilon_0 (\chi^{(1)} + 2\chi^{(2)} E_{dc} + 3\chi^{(3)} E_{dc}^2 + \frac{3}{4}\chi^{(3)} E_0^2) E_0 \cos \omega t \quad (4)$$

where χ_{eff} is the effective electric susceptibility and defined as

$$\chi_{eff} = \chi^{(1)} + 2\chi^{(2)} E_{dc} + 3\chi^{(3)} E_{dc}^2 + \frac{3}{4}\chi^{(3)} E_0^2 . \quad (5)$$

The refractive index, n, is expressed as

$$n^2 \approx K_{eff} = 1 + \chi_{eff} = n_0^2 + 2\chi^{(2)} E_{dc} + 3\chi^{(3)} E_{dc}^2 + \frac{3}{4}\chi^{(3)} E_0^2 + \cdots . \quad (6)$$

where K_{eff} is the effective dielectric constant and $n_0 = \sqrt{1+\chi^{(1)}}$ is the linear refractive index.

In general, the high order nonlinear coefficients are relatively smaller than the linear coefficient, thus Eq. (6) leads to the following relationship,

$$n = n_0 \left[1 + \frac{1}{n_0} \left(2\chi^{(2)} E_{dc} + 3\chi^{(3)} E_{dc}^2 + \frac{3}{4}\chi^{(3)} E_0^2 \right) \right]^{1/2} \approx n_0 + \frac{\chi^{(2)} E_{dc}}{n_0} + \frac{3\chi^{(3)} E_{dc}^2}{2n_0} + \frac{3\chi^{(3)} E_0^2}{8n_0} . \quad (7)$$

by the binominal expansion and approximation.

Therefore, the refractive index change, Δn, induced by the strong external DC field, E_{dc} ($>>E_0$), is given by

$$\Delta n = n - n_0 \approx \left(\chi^{(2)} + \frac{3\chi^{(3)} E_{dc}}{2} \right) \frac{E_{dc}}{n_0} . \quad (8)$$

It is noted that the first term, $\chi^{(2)}$, is zero in glass, therefore, the second term related to the third-order nonlinearity as well as the DC electric field only survives and results in,

$$\Delta n \approx \left(\frac{3\chi^{(3)} E_{dc}}{2} \right) \frac{E_{dc}}{n_0} = \frac{\chi_{eff}^{(3)} E_{dc}}{2 n_0} , \quad (9)$$

where the effective second-order nonlinear coefficient, $\chi_{eff}^{(2)}$, is defined as

$$\chi_{eff}^{(2)} = 3\chi^{(3)} E_{dc} . \quad (10)$$

This indicates that the second-order nonlinearity can be induced by introducing the DC electric field through the third-order nonlinear property of glass, $\chi^{(3)}$.

1.2 Characteristics of the silica fiber-based electro-optic devices

Characteristics of the silica glass fiber-based electro-optic devices were summarized in Table 1 and were compared with those of the $LiNbO_3$-based electro-optic devices.

There are several advantages in the silica glass fiber-based electro-optic devices. At first, optical connection between the fiber-based electro-optic devices and other fiber-based components is easily carried out by the simple fusion splicing technique and this diminishes the increase in the production cost typically arisen from the time consuming packaging process for optical alignment. The splicing loss can be decreased to the neglected level, ~0.1 dB, since the refractive index of the devices is well matched with other fiber devices. Optical

Table 1. Comparison of the Characteristics Between the Silica Glass Fiber-based and the $LiNbO_3$-based Electro-optic devices[16].

Property	$LiNbO_3$-based (commercial)	Silica fiber-based (prototype)
Refractive index (at 1550 nm)	2.21 (n_o) 2.13 (n_e)	1.46 (GeO_2: ~13 mol %)
Refractive index (at RF frequency)	5.4	2.0
SON coefficient $\chi^{(2)}$ (pm/V)	~60 (χ_{33}), ~7(χ_{21}) at 633 nm	0.2-0.5 at 1550 nm
Absorption coefficient of material	~0.2 dB/cm	~1 dB/km
Bandwidty (GHz)	40	0.1
Insertion loss (dB)	4	<2
Extinction ratio (dB)	>20	>20
Driving voltage (Vπ)	5-10	100-300
Vπ · L (V · cm)	~10	~5000

loss of silica glass itself is also negligibly small in comparison with that (~0.2 dB/cm) of $LiNbO_3$.

In the $LiNbO_3$-based electro-optic devices, on the other hand, the considerable insertion loss (typically more than 4 dB) is induced due to the refractive index mismatch when the devices are with the conventional silica-based optical fibers. Furthermore, time consuming optical aligning procedure is essential for optical packaging of the $LiNbO_3$-based device and this makes considerable increase in device cost.

It is another advantage for the silica-based electro-optic devices that the cost of silica glass is much cheaper than that of the nonlinear crystal, $LiNbO_3$. Moreover, a number of the waveguide fabrication steps can be reduced into the relatively simplified procedures in the case of the silica glass fiber-based devices. These advantages make the cost effectiveness in fabrication of the silica glass fiber-based electro-optic devices.

However, the electro-optic effect of silica glass is 2 orders of magnitude smaller than that of $LiNbO_3$ even after glass poling to enhance the second-order nonlinearity. The small nonlinearity of the fiber makes the fiber-based device use the long electrode with ~ 100 cm, or the large driving voltage, ~ 100V. Unfortunately, this also forces to the increase in the volume of the device and the decrease in the modulation speed. Therefore, it is essential to enhance the second-order nonlinearity of the fiber by optimization of the fiber core composition and the glass poling process.

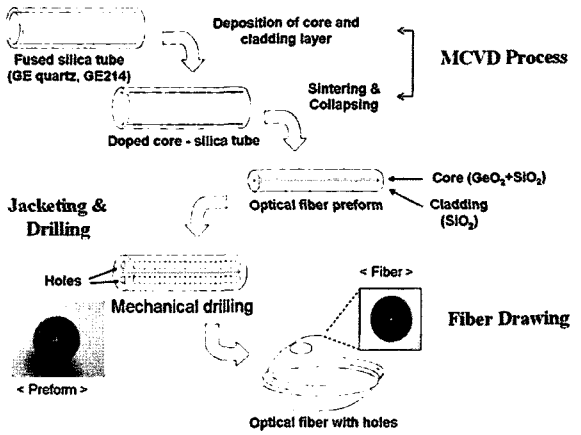

Fig. 1. Fabrication procedure of the optical fiber with holes for electro-optic applications[16].

2. Fabrication of the Electro-optic Fibers

2.1 Fabrication of the glass optical fibers with holes

The schematic fabrication procedure of the optical fiber with holes for electro-optic applications is shown in Fig. 1. Optical fiber preforms with core and cladding layers were made by the MCVD process[17].

Fused silica glass tubes (GE Quartz, code # 214) were used as the substrate material for the fiber preforms. The concentrations of OH, Na, Li, and K, impurities of the silica glass tube, were < 5, 0.7, < 0.1, and 0.6 ppm by weight, respectively[18]. Fine soots for the inner cladding and the core layers were deposited inside the silica tube by the reactions of SiCl4, $GeCl_4$, $POCl_3$, and CF_4 with O_2 gas at high temperature, ~ 2000 ℃. Then optical fiber performs were fabricated by the subsequent sintering and collapsing processes. The performs were jacketed with the silica glass tube to satisfy single mode condition by adjusting the diameter ratio between the core and the cladding.

Then, two holes with the diameter of 4-5 mm were made at both sides of the core of the fiber preform using a mechanical drilling machine. Finally, the performs were drawn into optical fibers with the outer diameter of ~125 μm by control the drawing temperature and the speed to preserve the holes during the process. As a result, the optical fibers with different core compositions and dimensions were obtained as shown in Table 2. The Fibers A1 and A2 were made by the Ge-

doped preform with the low Ge concentration (~3.2 mol%), on the other hand, the nearest distance between the core center and the hole boundaries (CHD) and the nearest distance between the hole boundaries (HD) were different in the fibers since the drilled positions of

Table 2. Specifications of the Optical Fibers with Two Holes

Fiber	Δn	Core shape	CHD	HD
			μm	μm
A1	0.0046	circular	10.3	34.9
A2			14.6	39.7
B1	0.0179	circular	10.4	31.5
B2		elliptic	11.2	36.7

* Δn means the refractive index difference between the core and the cladding of the fiber.

the holes were different each other. The Fibers B1 and B2 were made by the Ge-doped preform with the high Ge concentration (12.1 mol%), on the other hand, CHD and HD were different since the circular and the elliptic cores were made for the Fibers B1 and B2, respectively, by the control of drawing condition.

2.2 Formation of the internal electrodes in the optical fibers

Electrodes with appropriate electrical, thermal, and mechanical characteristics are needed to apply electric field to the optical fibers. The electrode material was selected to have the higher melting temperature than the temperature for glass poling, ~ 250 ℃. The electrodes should be mechanically strong and long enough for practical modulation devices, for example 70 cm in length for an electro-optic modulator[5], since the long active length can compensate the small second-order nonlinearity of the glass fiber. The distance between the electrodes should be close enough to operate with the small driving voltage. In practical aspects, capability on fusion splicing between the electro-optic fiber with the conventional optical fiber is another requirement to prevent time consuming optical connection process. Therefore, the electrodes at the fiber ends should be removed before fusion splicing for optical connection. Several methods have been established to make electrodes inside the fibers using the side polishing[19,20], the manual insertion[21], and the in-line conducting wire drawing processes[22].

In the present study, two types of alloy metals, 37%Pb-63%Sn and 80%Au-20%Sn, were used as the electrode and the molten alloy injection technique[23] was used to form electrodes inside the holes of the fibers. The schematic of the electrode injection of the molten metal alloys by use of the pressure chamber to form the electrodes inside the twin holes of the fibers is shown in Fig. 2. Alloys with different compositions were injected into the holes of the fibers by the aid of nitrogen gas at 10-15 bar after being melted by an electric furnace. As a result, optical fibers incorporated with the continuous and long internal electrodes were successfully made with the length more than 1 m.

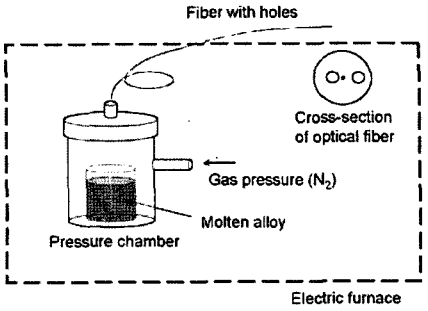

Fig. 2. Schematic of the internal electrodes formation by injection of the molten metal alloys[23].

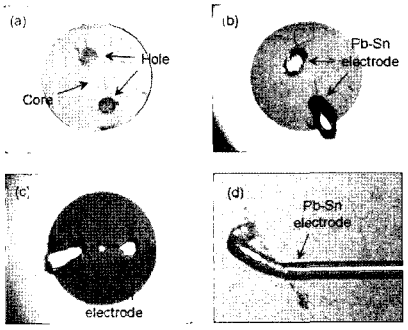

Fig. 3. Cross-sectional photographs of the optical fiber (Fiber A2) with holes (diameter, 20 μm) (a) before and after formation of (b) 37%Pb-63% and (c) 80%Au-20%Sn electrodes by the molten alloy injection technique. (d) is the side view of the fiber with 37%Pb-63%Sn electrode[10,16].

Fig. 3 shows the cross-sections of the fiber before and after the formation of the internal electrodes in the Fiber A2. As shown in the figure, the electrodes with the metallic luster are found to be formed inside the holes of the fiber.

For electric contact between electric devices and the internal electrodes of the fiber, the side surfaces

of the fibers were polished using abrasive pads (grade P-2000, 2400) for several minutes. The electrodes outcropped by the polishing were connected with the power port of the electric devices using the conductive silver epoxy. To protect the fiber from mechanical breakage, the fiber was molded into the grooved silica block before the polishing procedure.

Electric resistance of the electrodes was investigated after the electric contact procedure. The measured electric resistances of the electrodes with the diameter of 24.3 μm for the 80%Au-20%Sn and 37%Pb-63%Sn compositions were ~5.5 and ~2 Ω/cm, respectively[16].

2.3 Characterization of the fibers with the internal electrodes

The small insertion loss and the large second-order nonlinearity of electro-optic fibers are important characteristics to determine the quality of the electro-optic devices. Thus, optical transmission spectra of the optical fibers with different refractive index differences and distances between the core and the electrode were investigated before and after the formation of internal electrodes[10,16]. The transmission spectra were measured by the optical spectrum analyzer (Ando, AQ-6315B) and the white light source (Ando, AQ-4303B). The internal electrode lengths of the fibers under test were in the range, 94-97 cm, and the length of the fibers with electrodes was fixed at 100 cm. For the measurement, normal 100 cm long Ge-doped single mode fibers were connected to the fibers at both sides using the fusion splicer. As a reference, the transmission spectra of the fibers without the internal electrodes were also measured.

Fig. 4 shows the transmission spectra of the Fibers A1 and A2 with the different distances between the core center and the nearest boundary of the electrodes (CEDs), which is equals to CHD defined in Table 2. The transmission

spectra with the electrodes were compared with that without the electrodes. As shown in the figure, the transmission spectra of the fiber without electrodes slightly decreased with the increase of wavelength. In the case of the electrodes with the CED of 10.3 μm, on the other hand, the transmission considerably decreased with the increase of wavelength. It is known that optical loss is induced by light absorption at the surface of conducting materials[24,25]. Thus, the larger optical loss in the fibers with the electrodes is considered to be due to optical absorption by electrodes near the core. The larger optical loss was induced at longer wavelength because of the smaller optical confinement in the core at the wavelength. The electrode induced optical loss (EIL) of the fiber was estimated to be 47.4 dB/m at 1550 nm. In the case of the fiber with the larger CED of 14.6 μm, the relatively smaller EIL of 10.7 dB/m was found at 1550 nm because of the larger distance between core and the electrodes.

Dependence of EIL on the refractive index difference between core and cladding was investigated. The EIL by 37%Pb-63%Sn electrodes were found to be 14.0 and 6.7 dB/m at refractive index differences of 0.0124 (CED, 10.9 μm) and 0.0179 (CED, 10.4 μm), respec-

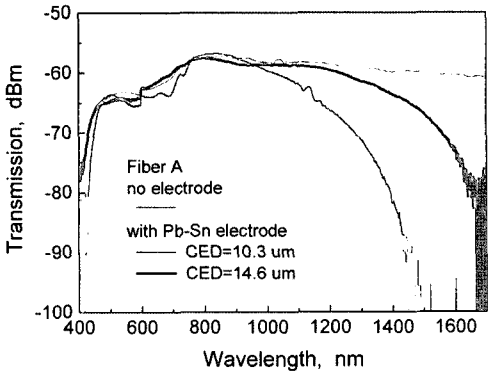

Fig. 4. Optical transmission spectra of the Ge-doped fiber (Fiber A) with and without the internal 37%Pb-63%Sn electrodes. The lengths of all fibers were 100 cm and the internal electrodes lengths were 95 cm.[10,16].

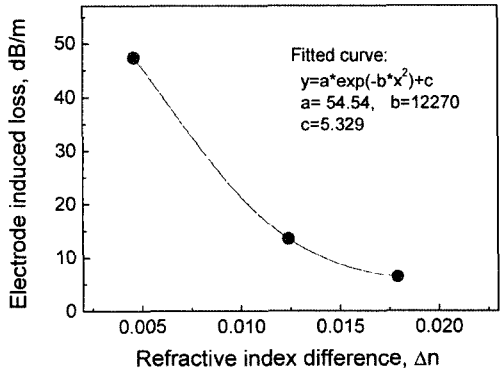

Fig. 5. Electrode induced loss by 37%Pb-63%Sn electrodes with the refractive index difference between core and cladding. The CED was fixed at almost constant in the range, 10.3-10.9 μm[16].

tively[16].

Fig. 5 shows the measured EIL with the refractive index difference. It was found that EIL exponentially decreased with the increase in the refractive index difference. This is because the optical field was more

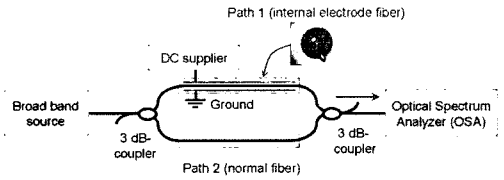

Fig. 6. Schematic setup for nonlinear optical characterization using the Mach-Zehnder interferometry[16].

strongly confined to the core region with the larger refractive index difference in the fibers.

Nonlinear optical characteristics of the electro-optic fibers were investigated by measurement of the electric-field induced optical phase shift using the Mach-Zehnder interferometer (MZI) configuration[10,16]. The schematic setup for the measurement is shown in Fig. 6.

A polarized light from the broad band light source (ThorLabs, SOA240) was injected into the input port of the MZI and was coupled into the two arms of the MZI after being divided by use of the 3-dB fiber coupler. One arm of the MZI was connected to the electro-optic fiber with internal electrodes as the active part and the DC voltage with the different magnitude was applied. For the other reference arm, the fiber without the electrodes was used. Due to phase changes after passing through each arms, the lights superimposed again at the second 3-dB fiber coupler and resulted in interference fringes in the optical spectra at the output. The change in the fringes was investigated by the OSA.

Fig. 7(a) shows the interference fringe shift induced by applying the electric voltage of 2.4 kV in the Fiber A2[16]. The resulted fringe shift was 2.4 nm to the longer wavelength and corresponded to the phase shift of ~π/2. The measured optical phase change with the different applied DC voltages was shown in Fig. 7(b). The phase was found to increase with the increase of the applied DC voltage in a parabolic form.

The electric-field induced parabolic phase shift can be explained by the refractive index change obtained from the electro-optic Kerr effect in the glass fiber as previously described in Sec. 1.1,

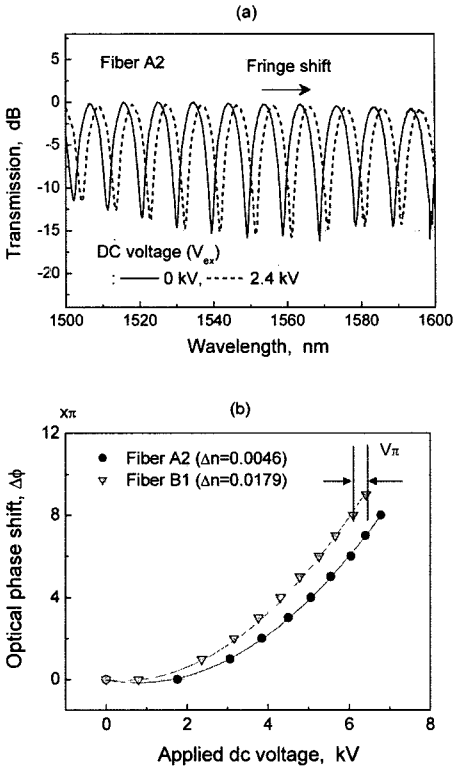

Fig. 7. (a) Interference fringe spectra of the Ge-doped fibers before and after applying the DC voltage of 2.4 kV and (b) optical phase shift with the applied DC voltage and the fitted curves [16].

$$\Delta n = n - n_0 \approx \frac{3\chi^{(3)}}{2n_0} E_{dc}^2 \cdot \tag{11}$$

Thus, the electric-field induced optical phase change, $\Delta\phi$, is given by

$$\Delta\phi = \frac{2\pi\,\Delta n\,L}{\lambda_0} = \frac{3\pi L\,\chi^{(3)}}{n_0\lambda_0 d^2} V_{dc}^{\,2}, \tag{12}$$

where L is the electrode length, d is the distance between the electrodes, λ_0 is the optical wavelength of light, and V_{dc} is the applied DC voltage. Eq. (12) indicates that the phase change depends on the square of the voltage and is determined by the third-order optical nonlinearity ($\chi^{(3)}$) and the design parameters (n_0, L, d) of the fiber. Thus, the third-order optical nonlinearity can be estimated from the measured phase shift and the known design parameters.

As shown in Fig. 7(b), the phase shifts with the applied DC voltage of the Fiber A2 (Ge concentra-

tion ~3.2 mol %) were well fitted by the shifted form of the parabolic equation, $y = a \cdot (x+b)^2+c$, where a, b, and c were equal to 0.2264, -0.7817, and -0.1628, respectively. The least square method was used for the fitting. The offset voltage, -0.7817 kV, was found and was considered to result from the weak poling at room temperature during the nonlinearity measurement. Thus, Eq. (12) can be modified into the following form,

$$\Delta\phi = \frac{2\pi\,\Delta n\,L}{\lambda_0} = \frac{3\pi L\,\chi^{(3)}}{n_0\lambda_0 d^2}(V_{dc}+V_{rec})^2, \qquad (13)$$

where V_{rec} is the recorded poling field. From the fitted curve and Eq. (11), the third-order optical nonlinearity was calculated to be 1.79×10^{-22} m^2/V^2. This is similar to the nonlinearity, $\chi^{(3)}=1.76\text{-}1.92\times10^{-22}$ m^2/V^2, of silica glass in the previous reports[26,27].

Phase shift with the DC voltage was also examined in the Fiber B1 with the higher Ge concentration, ~12.1 mol %. The parabolic characteristics in the phase shift was also found again in the fiber. The third-order optical nonlinearity of the fiber was calculated to be 2.00×10^{-22} m^2/V^2 and was slightly larger than that (1.79×10^{-22} m^2/V^2) of the Fiber A with the lower Ge concentration.

The half-wave voltages (V_π), defined as the voltage for π-phase shift, near the DC voltage of 6.3 kV were obtained to be 380 and 330 V in the Fibers A2 and B1, respectively. The half-wave voltage for the Fiber A was represented in Fig. 7(b) and it indicates that the voltage is pretty high as the driving voltage in comparison with the commercial electro-optic devices. Therefore, improvement of the electro-optic properties of the fibers by optimization of the core composition and the glass poling is essential to decrease the half-wave voltage to the commercial level, ~ 5-10 V.

The effective second-order nonlinearities of the fibers were also estimated from the measured third-order nonlinearities, 0.134 and 0.150 pm/V for the Fibers A and B, respectively. For the estimation, E_{dc}=250 kV/mm was used as the DC field.

3. Application of the Electro-optic Fibers

3.1 All-fiber electro-optic polarimetric modulation device based on the glass optical fiber with internal electrodes

Recently, an all-fiber electro-optic modulation device was demonstrated using the polarimetric cell based on the optical fiber with internal electrodes[10]. For the investigation, the electro-optic fiber (Fiber A2) with the Ge-doped core and the internal electrodes with electrode composition of 37%Pb-63%Sn was used. The electrodes were formed by the molten alloy injection technique as previously described in Sec. 2.2.

In Fig. 8, the schematic setup of the all-fiber polarimetric modulation device based on the electro-optic fiber was described. The length of the internal electrode was 149 cm. After its polarization state was controlled by the polarization controller (PC), 1550 nm-polarized light with the optical power of 5 mW from the tunable laser source (Santec, TSL-200) was injected into the fiber. Then the light passed through the internal electrode fiber and the linear polarizer. The optical power of the light was finally detected by the photo-receiver. Two PCs were used to align the input polarization state of the light and the polarizer with respect to the principal axes of the internal electrode fiber at 45°. The principal axes of the fiber correspond to the polarization directions of light parallel and perpendicular to the direction of the external electric field.

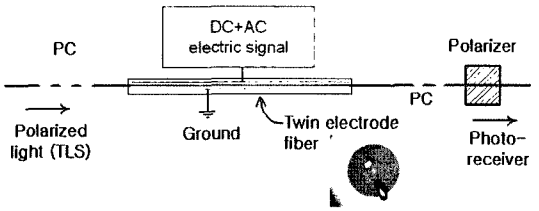

Fig. 8. Schematic setup of the all-fiber polarimetric modulation device made by the optical fiber with Pb-Sn internal electrodes[10].

At first, effect of the applied DC voltage on the modulation characteristics of the optical signal was examined in the polarimetric device. Fig. 9 shows the optical signal with the different biased DC voltages superimposed on the modulation AC signal with the constant peak-to-peak voltage of 560 Vpp. The modulation frequency of the AC signal was also fixed at 20 kHz.

At zero DC voltage, no optical signal was found as shown in Fig. 9 since there was no initial birefringence in the fiber and the intensity of the AC voltage was too small to make optical modulation by inducing the birefringence without the intense DC voltage. On the other

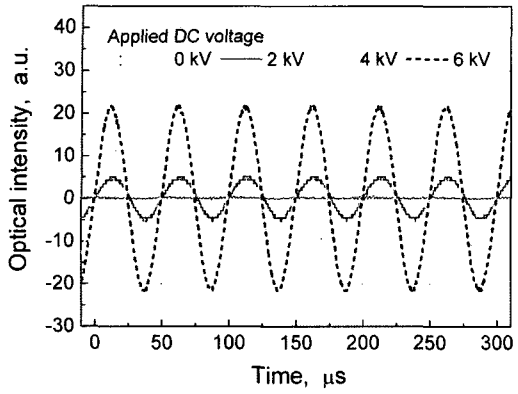

Fig. 9. Modulated optical signal of the all-fiber polarimetric modulation device applied with the different DC bias voltages in the range, 0 - 8 kV. The peak-to-peak intensity and frequency of the AC modulation voltage were fixed at 560 Vpp and 20 kHz, respectively[10].

hand, the clear optical signals were found at the higher DC voltages and the modulation intensity increased with the increase of the DC voltage. The frequency of the optical modulation was well matched with the applied modulation frequency, 20 kHz.

The optical modulation was explained by the generation of the initial phase retardation due to the electric-field induced birefringence by the applied DC voltage and the additional modulation of the retardation by the AC signal as follows[10].

In an isotropic media under an external DC electric field, the effective second-order nonlinear coefficient, $\chi^{(2)}_{eff}$, by the electro-optic Kerr effect has polarization dependence as[28,29]

$$\chi^{(2)}_{eff,\,TM} / \chi^{(2)}_{eff,\,TE} = \gamma \neq 1 \tag{14}$$

where the subscripts of TM and TE indicate the polarization directions of the light parallel and perpendicular to the direction of the applied electric field, respectively. The γ indicates the ratio of the effective second-order nonlinear coefficients between the two polarization directions.

If the TM polarization term is taken as $\Delta n_{TM} = \chi^{(2)}_{eff}$, $_{TM}E/(2n_0) = 3\chi^{(3)}E^2/(2n_0)$, the TE polarization term is given by $\Delta n_{TE} = \chi^{(2)}_{eff}$, $_{TE}E/(2n_0\gamma) = 3\chi^{(3)}E^2/(2n_0\gamma)$from Eqs. (9) and (11) with the assumption that the third-order nonlinear coefficient is independent of the polarization direction. Thus, the optical transmittance, T, of the all-fiber polarimetric modulation device with the retardation due to the electro-optic Kerr effect resulting from applied external field is given by[10]

$$\begin{aligned} T &= \sin^2(\Gamma/2) \\ &= \sin^2\left[\pi(n_{TM} - n_{TE})L/\lambda_0\right] \\ &= \sin^2\left[\frac{\Gamma_0}{2} + \frac{3\pi L(1-1/\gamma)\chi^{(3)}}{2n_0\lambda_0 d^2}\cdot V^2\right] \end{aligned} \tag{15}$$

where Γ is the total retardation, Γ_0 is the retardation from the birefringence of structural asymmetry of the fiber and the polarization controller, L is the electrode length, λ_0 is the optical wavelength, d is the distance between the electrodes, and $V(=E \cdot d)$ is the applied the external electric potential.

If the small AC electric signal, dV, in comparison with the larger DC voltage is applied, the modulation, dT, in optical transmittance is given by[10]

$$dT = \frac{3\pi L(1-1/\gamma)\chi^{(3)}}{n_0\lambda_0 d^2}\sin\left(\Gamma_0 + \frac{3\pi L(1-1/\gamma)\chi^{(3)}}{n_0\lambda_0 d^2}\cdot V^2\right)\cdot V\cdot dV. \tag{16}$$

From the equation, the optical modulation intensity is proportional to the modulation magnitude of the applied electric field and the third-order nonlinearity, $\chi^{(3)}$. Thus, the use of a material with high third-order nonlinearity is needed to obtain high performance in the electro-optic devices operated at small driving voltage.

The optical modulation characteristics were examined by changing the frequency of the applied AC signal in the range 1-50 kHz[10]. For the investigation, the peak-to-peak intensity of the AC voltage and the biased DC voltage were maintained at the constant 560 Vpp and 5 kV, respectively.

The resulted optical signals with the different modulation frequencies are shown in Fig. 10. As shown in Fig. 10(a), it was found that the tuning of the optical modulation frequency was very stable and the periodicity of the optical modulations was well matched to the modulation frequency of the applied AC signal. Fig. 10(b) shows the peak-to-peak intensity of the optical signal with the frequency of the AC signal in the range, 1-55 kHz. The modulation intensity of the optical signal was found to be almost constant in the frequency range with the fluctuation smaller than ± 4.5 %.

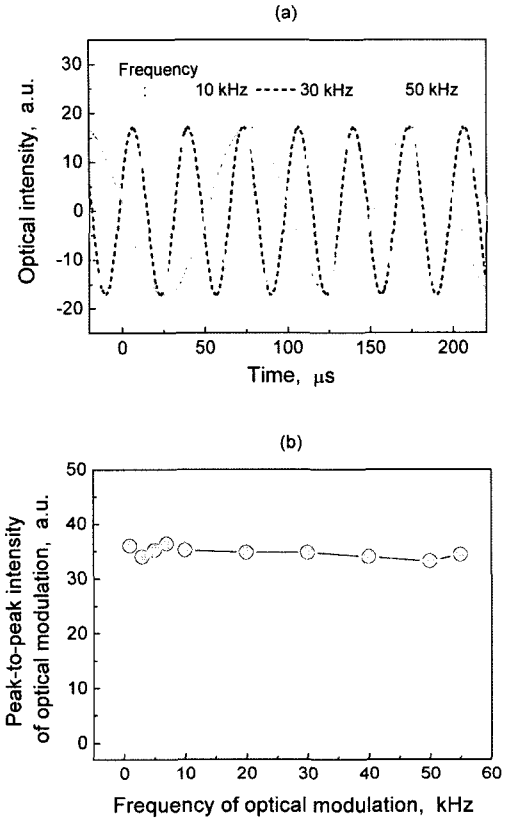

Fig. 10. (a) Modulated optical signals with the modulation frequencies of 10, 30, and 50 kHz and (b) peak-to-peak intensity of the optical signal with the frequency of the AC signal in the all-fiber polarimetric modulation device. The peak-to-peak intensity of the AC voltage and the biased DC voltage were fixed at constant 560 Vpp and 5 kV, respectively[10].

Recently, an all-fiber modulation device made by Sagnac fiber-loop interferometer (SFLI) based on an electro-optic fiber was demonstrated[11], in which the same electro-optic fiber (Fiber A2, electrode length ~149 cm) was used for the active part in the fiber loop. It was found that the optical modulation with the shape and the frequency matched with those of the applied electric signal was obtained. The frequency response of the modulation was also tested in the frequency range, 5-50 kHz. The intensity of the optical modulation was found to be stable in the range with the fluctuation smaller than ± 7 %. The modulation characteristics were very similar to those of the polarimetric device shown in Fig. 8. This is because the device has the same form of the transmittance function given by Eq. (15)[10,16]. That is, the same wave retarder was used as an active part that makes the optical modulation by changing the polarization state.

In general, the SFLI has advantages such as the insensitivity to the input polarization state, the large extinction ratio, and the large optical tunability[30,31]. Therefore, the all-fiber modulation device using the SFLI have potentials for the applications on wavelength division multiplexing, optical switching /modulation, and wavelength tuning in fiber optic systems.

3.2 Electro-optic tuning device based on the glass optical fiber with internal electrodes and a birefringent elliptic core

In the previous section, electro-optic modulation devices with the all-fiber polarimetric cell made by the internal electrode fiber with a circular core were reviewed. Recently, another all-fiber electro-optic device based on polarimetric cell was also investigated by use of the optical fiber with the elliptic core[12,16].

For the investigation, the same optical fiber preform with a Ge-doped core for the Fiber B1 was used to make the fiber with the elliptic core. The optical fiber (Fiber B2) with the elliptic core was made by the MCVD, drilling, and fiber drawing processes. The cross-sectional sizes of the core were ~3.9 and ~6.5 μm in the short and long axes, respectively. To introduce 63%Sn-37%Pb electrodes in the holes of the fiber the molten alloy injection technique was used. As a result, an optical fiber with the continuous internal electrodes with the electrode length of 142 cm was obtained.

In Fig. 11, the photographs of the cross-section of the optical fiber with the birefringent core before and after the formation of the electrodes are shown. The

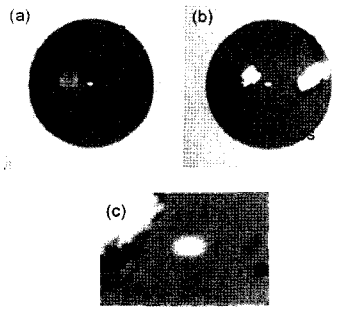

Fig. 11. Photographs of the optical fiber cross-section with the elliptic core (a) before and (b) after the formation of the 37%Pb-63%Sn electrodes and (c) the magnified view of the core region[12,16].

elliptic core was found to locate at the center of the fiber with the alloy electrodes.

Fig. 12 shows the schematic of the electro-optic tuning device made by a SFLI based on the electro-optic fiber. For the SFLI, the 202 cm-long elliptic core fiber with 142 cm-internal electrodes was connected into the

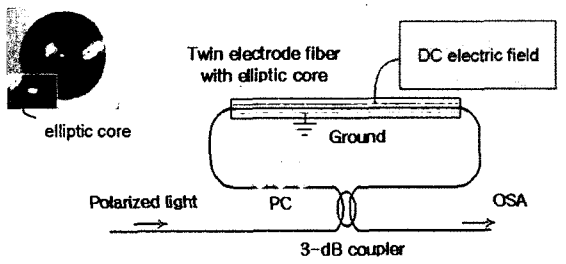

Fig. 12. Schematic setup of the all-fiber electro-optic tuning device made by a SFLI based on the optical fiber with an elliptic core and internal electrodes[12].

loop made by the 3-dB fiber coupler.

The transmission spectra of the SFLI made by the electro-optic fiber with and without the internal electrodes were investigated[12]. The polarized light from the broad band source (ThorLab, SOA240) was coupled into the input port and the optical spectra at the output port were measured using the OSA (ANDO, AQ6315B).

Fig. 13 indicates the transmission spectra of the SFLI with and without the internal electrodes. The transmission spectrum of the normal single mode fiber (n-SMF) was also represented as a reference. In the SFLI without the electrodes, the clear interference fringes were found with the extinction ratio larger than 15 dB in all spectral regions and the fringe spacings of 8.64 and 10.28 nm at 1310 and 1550 nm.

It is known that the transmittance of the SFLI has the power variation with the wavelength period of[30,31]

$$S = \frac{\lambda^2}{\Delta n_b L} \tag{17}$$

, where Δn_b is the modal birefringence, L is the length of the birefringent fiber, and λ is the optical wavelength. The period of the bandwidth depends on the wavelength, the modal birefringence, and length of the fiber in the SFLI. From the measured fringe spacings, Δn_b of the fiber were calculated to be 9.83×10^{-5} and 1.16×10^{-4}, respectively, using Eq. (17).

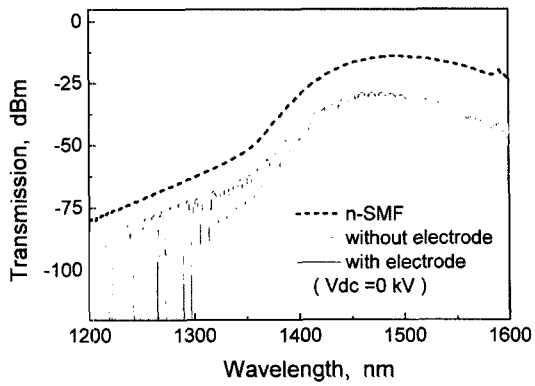

Fig. 13. Transmission spectra of the SFLI based on the electro-optic fiber with the birefringent elliptic core with and without the internal electrodes[12].

In the transmission spectrum of the SFLI with the internal electrodes, the intensity of the fringe became smaller with the increase of the wavelength and almost disappeared near 1550 nm. The difference between the transmission spectra with and without the electrodes can be explained by the polarization dependent optical absorption at the surface of the conducting electrodes. The mode field diameter is larger at longer wavelength and light polarized in the parallel direction of the electrode surface is heavily absorbed. Therefore, the fringes at longer wavelength disappeared.

The electro-optic characteristics of the SFLI were examined by applying the different DC electric voltages in the range, 0-10.1 kV[12]. The tuning of the interference fringe of the SFLI was found to be induced by applying the voltage as shown in Fig. 14. The transmission spectra of the SFLI at the DC voltage of 0 and

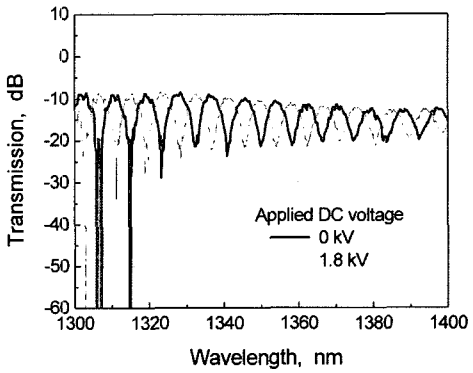

Fig. 14. Transmission spectra of the SFLI based on the electro-optic fiber with the birefringent elliptic core at the DC voltages of 0 and 1.8 kV[12].

1.8 kV were presented after being referenced by the transmission of n-SMF. The fringe shift of -4.26 nm corresponding to π-phase shift was induced by applying the DC voltage of 1.8 kV.

Fig. 15 shows the interference fringe shift near 1350 nm and the corresponding modal birefringence change with the applied DC voltage. The fringe was found to shift to the shorter wavelength with the increase of

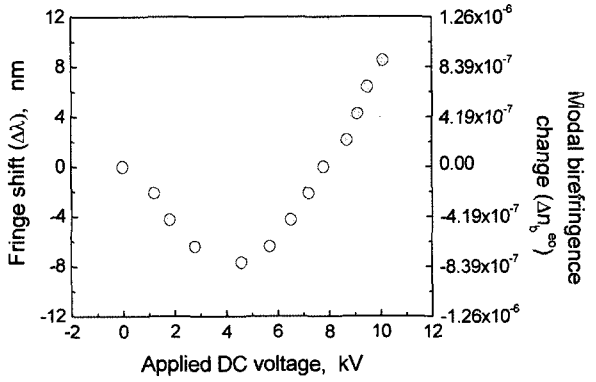

Fig. 15. Interference fringe shift of the SFLI and the electric field induced modal birefringence change with the DC voltage in the range, 0-10.1 kV[12].

the voltage and reached the minimum shift, 7.7 nm, at 4.6 kV, then shifted to the longer wavelength with the further increase of the voltage and finally reached to the maximum shift, 8.52 nm, at 10.1 kV. Interestingly, the tuning characteristics was different from that of the MZI. In the case of the MZI, the fringe shift monatonically increased in proportion to the square of the DC voltage as shown in Fig. 7.

The electro-optic tuning characteristics can be explained by the electric-field induced modal birefringence change due to the electro-optic Kerr effect. The transmittance, T, of the SFLI made by the birefringent fiber with the linear birefringence, δ, is given by[30,31]

$$T = \sin^2(\delta/2) \tag{18}$$

$$\delta = 2\pi\Delta n_b L/\lambda \tag{19}$$

where $\Delta n_b = n_{TM} - n_{TE}$ is the modal birefringence, L is the length of the birefringent fiber, and λ is the optical wavelength. The subscripts of TM and TE indicate the polarization directions of light to the directions of the long and short axes of the core, that are equal to the parallel and perpendicular directions of the applied electric field, respectively.

From the electric-field induced interference fringe shift, the modal birefringence change in the partial length, L^{eo}, can be estimated using the phase term, $\phi = \delta/2$.

$$\phi_1 = \pi\Delta n_b L/\lambda \tag{20}$$

In the equation, ϕ_1 indicates a specific phase when the electric field is zero. When the electric field is applied, the electric field induces the fringe shift, $\Delta\lambda$, due to the modal birefingence change, Δn_b^{eo}, and the phase term with the electric field is given by

$$\phi_2 = \pi(\Delta n_b L + \Delta n_b^{eo} L^{eo})/(\lambda+\Delta\lambda) \cdot \tag{21}$$

By considering the same phase terms, $\phi_1 = \phi_2$, with and without the electric field, the modal birefringence change is expressed as[12]

$$\Delta n_b^{eo} = \frac{\Delta n_b L}{\lambda L^{eo}} \Delta\lambda \cdot \tag{22}$$

Therefore, the electric-field induced modal birefringence change can be calculated from the fringe shift, $\Delta\lambda$, using the equation. As a result, the fringe shift of -4.26 nm at 1.8 kV was calculated to be induced by the modal birefringence change, -4.46x10-7. The modal birefringence change reached to the lowest value of -8.03×10^{-7} at 4.6 kV, and turned to increase with the increase of the applied DC voltage and finally reached to 8.92×10^{-7} at 10.1 kV.

4. Conclusion

The fabrication and the several applications of glass optical fibers were reviewed for all-fiber electro-optic devices.

Theoretical background on the electro-optic Kerr effect in glasses was described to explain second-order nonlinearity in glass fibers. The fabrication processes of the fibers with internal electrodes by the MCVD, the mechanical drill, the fiber drawing, and the electrode formation processes were also described.

It was found that the optical attenuation increased in the fibers with the electrodes and the increase was explained to be due to light absorption at the surface

of the metal electrodes. As for the nonlinear optical characteristics of the fibers investigated using a MZI, the parabolic characteristics in the optical phase shift was found to be due to the electro-optic Kerr effect. The third-order optical nonlinearity was obtained to be 1.79-2.00 $\times 10^{-22}$ m^2/V^2 in the Ge-doped fibers and the effective second-order optical nonlinearity was estimated to be 0.134-0.150 pm/V in the fibers.

Based on our recent studies, several all-fiber electro-optic devices made by the polarimetric cells based on the optical fibers with the internal electrodes were also discussed.

An electro-optic modulation device was made by the polarimetric cell based on the electro-optic fiber with a circular core and internal 37%Pb-63%Sn electrodes. It was found that the optical modulation was stable in the frequency range, 1-55 kHz. Electro-optic tuning characteristics of the SFLI made by the optical fiber with an elliptic core and internal 37%Pb-63%Sn electrodes were demonstrated. The fringe shift of -4.26 nm, corresponding to π-phase shift, was induced by the electric-field induced modal birefringence change of 8.92×10^{-7} due to the applying electric field.

As a summary, the experimental results showed that the all-fiber devices based on the polarimetric cells made by the electro-optic fibers have large potentials for the applications on optical switching, modulation, and wavelength tuning in optical systems. However, more improvement of electro-optic properties of the fibers by optimization of core composition and glass poling is needed to decrease the operating voltage from several hundreds volts to the commercial level, ~ 5-10 V.

Acknowledgement

The authors thank S. Moon and A. Lin in GIST, Korea, for the fabrication of the optical fibers and S. Fleming in University of Sydney, Australia, for valuable comments on the electro-optic characterization of the optical fibers. This research was partially supported by Korea Science and Engineering Foundation through Ultrafast Fiber-Optic Networks (UFON), an Engineering Research Center program of GIST, by the National Core Research Center (NCRC) for Hybrid Materials Solution of Pusan National University, and by the Brain Korea-21 Project, Ministry of Education and Human Resources Development, Korea.

References

1. U. Osterberg and W. Margulis, "Dye laser pumped by Nd:YAG laser pulses frequency doubled in a glass optical fiber," Opt. Lett. vol. 11, pp. 516-518 (1986).
2. R. A. Myers, N. Mukherjee, and S. R. J. Brueck, "Large second-order nonlinearity in poled fused silica," Opt. Lett. vol. 6, pp. 1732-1734 (1991).
3. T. Fujiwara, D. Wong, and S. Fleming, "Large electrooptic modulation in a thermally-poled germanosilicate fiber," IEEE Photon. Technol. Lett. vol. 7, pp. 1177-1179 (1995).
4. T. Fujiwara, D. Wong, Y. Zhao, S. Fleming, S. Poole, and M. Sceats, "Electro-optic modulation in germanosilicate fibre with UV-excited poling," Electron. Lett. vol. 31, pp. 573-575 (1995).
5. N. Myren and W. Margulis, "All-fieber electrooptical mode-locking and tuning," Opt. Lett. vol. 17, pp. 2047-2049 (2005).
6. W. Margulis and N. Myren, "Progress on fiber poling and devices," in Technical digest of Optical Fiber Communication Conference 2005 (Optical Society of America, 2005) p. 3.
7. O. Tarasenko, N. Myren, W. Margulis, and I. C. S. Carvalho, "All-fiber electrooptical polarization control," in Technical digest of Optical Fiber Communication Conference 2006 (Optical Society of America, 2006) paper OWE3.
8. M. Abe, T. Kitagawa, K. Hattori, A. Himeno, and Y. Ohmori, "Electro-optic switch constructed with a poled silica-based waveguide on a Si substrate," Electron. Lett. vol. 32, pp. 893-894 (1996).
9. F. Garcia, L. Vogelaar, and R. Kashyap , "Poling of a channel waveguide," Opt. Express vol. 11, pp. 3041-3047 (2003).
10. B. H. Kim, S. Moon, U. C. Paek, and W.-T. Han, "All fiber polarimetric modulation using an electro-optic fiber with internal Pb-Sn electrodes," Opt. Express vol. 14, p. 11234 (2006).
11. B. H. Kim, S. Moon, U. C. Paek, and W.-T. Han, "All fiber electro-optic modulation using a Sagnac fiber-loop with an internal twin-electrode fiber," in technical digest of OptoElectronics and Communications Conference (Taiwan, 2006) paper 3P-008-1.
12. B. H. Kim, S. Moon, M. J. Kim, B. H. Lee, and W. -T. Han, "Electro-optic tuning in a Sagnac fiber-loop made by an internal twin-electrode fiber with a bire-

fringent core," in technical digest of Photonics Conference (Korea, 2006) p. 348.
13. B. H. Kim, H. Yang, A. Lin, and W.-T. Han, "Fabrication and characterization of an all-fiber electro-optic polarization controller based on an optical fiber with an elliptic core and internal electrodes," in technical digest of the Optical Society of Korea Annual Meeting 2007 (Korea, 2007), p. 40.
14. P. N. Prasad and D. J. Williams, Introduction to nonlinear optical effects in molecules and polymers (New York, John Wiley & Sons, 1990) chap. 1 and 4.
15. F. Agullo-Lopez, J. M. Cabrera, and F. Agullo-Rueda, Electrooptics (San Diego, Academic press, 1994) chap. 3 and 4.
16. B. H. Kim, "Development of second-order nonlinear optical waveguides and their applications to electro-optic devices," PhD dissertation, GIST, 2007.
17. J. B. MacChesney and P. B. O'Connor, U.S. Patent 4 217 027.
18. GE quartz catalog, Cleveland, USA.
19. M. -V. Bergot, M. C. Farries, M. E. Fermann, L. Li, L. J. Poyntz-Wright, P. St. J. Russell, and A. Smithson, "Generation of permanent optically induced second-order nonlinearities in optical fibers by poling," Opt. Lett. vol. 13, pp. 592-594 (1988).
20. P. G. Kazansky, L. Dong, and P. St. J . Russell, "High second-order nonlinearities in poled silicate fibers," Opt. Lett. vol. 19, pp. 701-703 (1994).
21. W. Xu, P. Blazkiewicz and S. Fleming, "Silica fiber poling technology," Adv. Mater. vol. 13, pp. 1014-1018 (2001).
22. K. Lee, P. Hu, J. L. Blows, D. Thorncraft, and J. Baxter, "200-m optical fiber with an integrated electrode and its poling," Opt. Lett. vol. 29, pp. 2124-2126 (2004).
23. M. Fokine, L. E. Nilsson, A. Claesson, D. Berlemont, L. Kjellberg, L. Krummenacher, and W. Margulis, "Integrated fiber Mach-Zehnder interferometer for electro-optic switching," Opt. Lett. vol. 27, pp. 1643-1645 (2002).
24. M. A. Ordal, L. L. Long, R. J. Bell, S. E. Bell, R. R. Bell, R. W. Alexander, Jr., and C. A. Ward, "Optical properties of the metals Al, Co, Cu, Au, Fe, Pb, Ni, Pd, Pt, Ag, Ti, and W in the infrared and far infrared," Appl. Opt. vol. 22, pp. 1099-1199 (1983).
25. R. K. Wangsness, Electromagnetic fields (New York, Wiley and Sons, 1986) chap. 10 and 11.
26. A. C. Liu, M. J. F. Digonnet, and G. S. Kino, "Measurement of the dc Kerr and electrostrictive phase modulation in silica," J. Opt. Soc. Am. B, vol. 18, pp. 187-194 (2001).
27. K. S. Kim, R. H. Stolen, W. A. Reed, and K. W. Quoi, "Measurement of the nonlinear index of silica-core and dispersion-shifted fibers," Opt. Lett. vol. 19, pp. 257-259 (1994).
28. S. Kielich, "Optical second-harmonic generation by electrically polarized isotropic media," IEEE J. Quantum Electron. QE-5, 562-568 (1969).
29. C. J. Marckmann, Y. Ren, G. Genty, and M. Kristensen, "Strength and symmetry of the third-order nonlinearity during poling of glass waveguides," IEEE Photon. Tech. Lett., 14, 1294-1296 (2002).
30. X. Fang and R. O. Claus, "Polarization-independent all-fiber wavelength-division multiplexer based on a Sagnac interferometer," Opt. Lett. vol. 20, pp. 2146-2148 (1995).
31. C.-S. Kim, Y.-G. Han, R. M. Sova, U. C. Paek, Y. Chung, and J. U. Kang, "Optical fiber modal birefringence measurement based on Lyot-Sagnac interferometer," IEEE Photon. Technol. Lett. vol. 15, pp. 269-271 (2003).